Combined influence of particle friction and inertia on hysteresis in granular media on an inclined plane

Clovis Lambert ,* Raphaël Maurin , Laurent Lacaze , and Pascal Fede

Institut de Mécanique des Fluides de Toulouse (IMFT), Université de Toulouse, CNRS, INPT, Université Toulouse III - Paul Sabatier (UPS), Toulouse, France

(Received 6 May 2024; accepted 10 February 2025; published 13 March 2025)

Understanding the transition between fluid-like and solid-like regimes of granular materials requires elucidating its hysteretic behavior. Yet, the origin of this hysteresis, defined as the difference in external stress necessary to induce flow or jamming of a granular medium, is still debated. While the origin of this hysteresis has long been attributed to grain's inertia, recent studies have shown that it depends on interparticle friction. To clarify the role of the different effects and possible interplays between them, we study the fluid-solid transition through three-dimensional discrete element simulations of dry and model-immersed granular flows down an inclined plane. In the dry case, a finite hysteresis is observed at the static-flowing transition even for frictionless particles. The hysteresis amplitude is shown to depend both on interparticle friction and particle inertia. Decoupling the effects of friction and inertia allows us to rationalize in a coherent picture the different results found in the literature. In particular, hysteresis is shown to become negligible when both friction and inertia are small, while it cannot be disregarded when at least one of them is present. The link between hysteresis amplitude and the discontinuous jump of compaction at the jamming transition is discussed. While the presence of hysteresis for frictionless particles is not associated with notable dilatancy and compaction at transitions, the coordination number exhibits discontinuous jumps at both transitions. Also, it is shown that the avalanche angle is directly linked to the static coordination number, and that the hysteresis amplitude is related to the coordination number discontinuity observed at jamming. These results highlight the strong link between the jamming-unjamming transition and the evolution of the granular microstructure through friction and inertia.

DOI: 10.1103/PhysRevFluids.10.034301

I. INTRODUCTION

Granular material has the particularity of solid-like and/or fluid-like behavior under various and complex loading stress or strain rates [1–4]. This specificity is characterized by critical yield stresses or strain rates that define criteria under which the medium is in the flowing or static state. This flowing-static transition is an important issue for the study of natural hazards such as snow avalanches or debris flows in landslides [5]. It is also an issue for applications such as pharmaceuticals and building or agriculture industries that use this solid-like or fluid-like behavior to produce, transport, extract, or store granular media [6–8].

Modeling this transition at the macroscopic scale still represents a challenge. In particular, although several constitutive models include hysteresis modeling [9–12], they do not describe the underlying physical mechanism responsible for the hysteretic behavior displayed by granular media at the transition. Indeed, For granular material in stress-imposed configurations, such as inclined

*Contact author: clovis.lambert@imft.fr

planes, rotating drums, or Couette cells, depending on the stress path, that is, the history of the stress applied to the medium, one can observe either a flowing or a static state at a given stress state [2,13–17]. This is well characterized for steady, uniform granular flow down an inclined plane, where the inclination angle sets the shear τ to normal P stress ratio $\tan(\theta) = \mu = \tau/P$ [18]. In this configuration, the inclination angle therefore sets the stress state of the granular medium. Starting from the flowing state above a critical inclination angle, the flow stops at a given angle θ_{stop}, which is smaller than the angle measured to initiate an avalanche θ_{start}, when increasing the inclination angle from the static state. This difference between the avalanche and stopping angle is characteristic of the hysteresis amplitude in the granular medium behavior.

Both critical angles, associated with critical global friction coefficients, similarly decrease when increasing the thickness of the flowing layer on an inclined plane. They have been shown to converge to a constant value that depends on the plane roughness when increasing the layer thickness toward a limit value of approximately 10 times the average diameter of grains [13,18]. This result shows that the finite size effect in the wall-normal direction is strong when the layer thickness is close to the particle diameter but saturates when the distance between the plane and the free surface of the medium is large enough.

Stopping and avalanche angles also similarly increase with interparticle friction [8,19,20], showing a strong effect of the sliding Coulomb criterion on the stability of the granular material. This effect saturates when the microscopic friction coefficient reaches approximately $\mu_p \approx 1$ [21]. Above this value, a granular medium enters the rolling regime in which all contacts respect the Coulomb criterion at the grain scale, leading to a constant effect of microscopic friction on granular stability [22].

The hysteretic nature of the transition, quantified by the difference between the avalanche and stopping angles, also varies with interparticle friction and layer thickness. Hysteresis relies on the combination of two different processes: the jamming, or cessation of flow, and the unjamming, or initiation of flow [8,13,17,23,24]. The initiation of flow from the static to a dense flow state is, in other words, a destabilization of the granular medium. Under shear stress or shear rate, a granular medium in the static state exhibits local rearrangements that are the local plasticity or fluidity of the granular material [24–26]. The characteristic size of these rearrangements increases with increasing imposed shear stress or shear rate. The size of these structures diverges when the granular medium is about to flow, leading to rearrangement of the order of the system size, destabilizing the assembly of grains that finally flows [24,27,28]. Besides, flow cessation or jamming has been extensively studied in the quasistatic limit of dense granular flow rheology and appears to be the result of the dissipation of the grains' motion by frictional and collisional contacts [17,22].

The physics of both the initiation and cessation of flow in granular media are particularly rich, such that most studies in the literature focus on one or the other phenomenon. Studying hysteresis at this transition requires considering the evolution of both phenomena as functions of relevant physical parameters. The nature of this hysteresis was first assigned to particle inertia effects [16,29] that prevent the flow from stopping when considering the arrest of a granular flow. Yet, more recent works [19–21,30,31] have shown that interparticle friction is a dominant mechanism in hysteresis at the expense of the inertia of grains. The framework that emerges from these works, proposed by DeGiuli and Wyart [21], assigned hysteresis behavior to the "self-fluidisation" of the granular medium in the flowing state. This process lowers the stress threshold, μ_{stop}, at which the medium stops compared with the one at which the medium starts flowing, μ_{start}. In this framework, the role of friction is central since the ability of the granular medium to "self-fluidise" is based on the idea that residual mechanical energy, that is, endogenous noise, due to collisions and network vibrations destabilizes contacts on the verge of sliding and then keeps in motion the whole assembly of grains. Hence, the ability of a tangential contact to be set in motion by this residual energy depends on the value of the coefficient of friction between the grains. This picture is supported by the fact that hysteresis amplitude depends on interparticle friction [19,20] and contact stiffness. Indeed, stiffness influences the residual energy and affects accordingly the hysteresis amplitude [21].

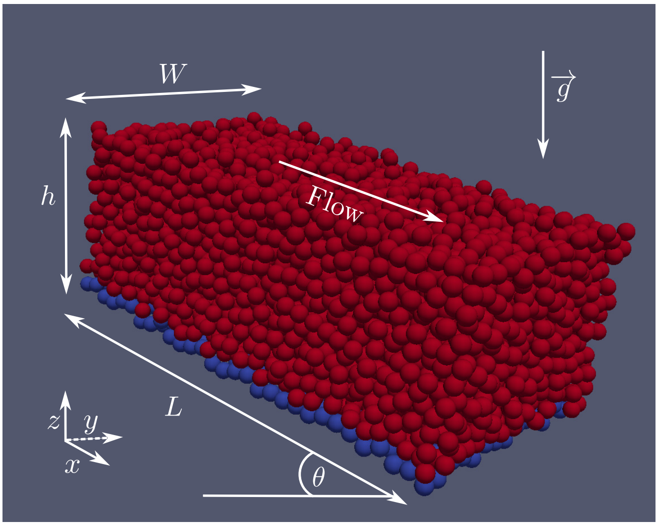

FIG. 1. Typical 3D snapshot of granular medium flowing on an inclined plane, $L \times W = 30d \times 15d$, $h = 10d$. Blue particles constitute the fixed rough plane, while red ones are free.

Based on these recent findings, some aspects remain to be elucidated. In particular, the vibrations induced by collisions are not canceled for frictionless material, and one expects the self-fluidization process to be partly present, even for frictionless particles. Since the experiments of Perrin *et al.* [20,31] are performed in the viscous Stokes limit, i.e., with negligible particle inertia and zero effective restitution coefficient, the residual energy is expected to be damped. This is incompatible with the self-fluidization process proposed by DeGiuli and Wyart [21] and suggests either that the latter is not appropriate or that it is canceled for low Stokes numbers and another mechanism is at work. In addition, the hysteresis amplitude obtained for frictional particles in Perrin *et al.* [20] is surprisingly high (of the same order as highly frictional dry materials with bumpy surfaces [19]), in particular considering the presence of a fluid damping the self-fluidization process.

In the present paper, hysteresis at the fluid-solid transition is studied on an inclined configuration by the mean of three-dimensional (3D) discrete element method simulations of dry and model-immersed granular media. This allows us to vary both interparticle friction and particle inertia independently. We show that frictionless granular media exhibit a finite hysteresis, contrary to what is expected. Going further, we show that the hysteresis amplitude depends on a combined effect of particle friction and inertia.

After detailing the simulation method, configuration, and framework in Sec. II, we qualitatively and quantitatively analyze the influence of the microscopic friction coefficient and grains' inertia on hysteresis in Sec. III. Then, we show that a microstructural description of the medium is needed to characterize well the discontinuity of the transition and unify the studies of both microscopic friction and inertia effect on hysteresis (Sec. IV).

II. SIMULATION METHOD AND DESCRIPTION OF CONFIGURATIONS

A. Configurations

The present study focuses on inclined plane simulation at the particle scale of cohesionless monodisperse spherical particles of diameter d forming a granular layer of size $h/d = 10$ (see Fig. 1). The layer thickness h, was selected to limit the computational time, considering the absence of a size effect above $h = 10d$ on the critical constraint ratio values [13,31]. We use a biperiodic domain of size $L \times W = 30d \times 15d$, L being the length in the streamwise direction and W in the spanwise direction (see Fig. 1). The choice of such domain size has been made with respect to a sensitivity analysis leading to a convergence of critical angles and hysteresis; see the Supplemental Materials [32] for a detailed analysis. The roughness of the plane is built using fixed particles, organized in a square paving in the streamwise and spanwise directions, with their wall-normal positions following a random uniform distribution between $-\frac{d}{2}$ and $\frac{d}{2}$. The code is made dimensionless, choosing d as the unit of length, $\sqrt{d/g}$ as the unit of time, g being the gravitational constant, and the mass of a grain m as the unit of mass. Note that in the following, the mass of a grain will always be replaced by $m = V_p \rho_p$ with the volume of a particle $V_p = \frac{\pi}{6} d^3$ and ρ_p the density of the grain.

The inclined plane configuration is considered with and without the influence of a surrounding fluid.

B. Discrete element method

The simulations are based on the discrete element method and performed using the open-source code YADE [33], where the motion of each particles is solved using Newton's second law for both translational and rotational motions

$$\frac{\pi}{6} d^3 \rho_p \frac{d\overrightarrow{u}}{dt} = \frac{\pi}{6} d^3 \rho_p \overrightarrow{g} + \sum_{i=0}^{N_c} \overrightarrow{F_{C,i}} + \overrightarrow{F_F}, \tag{1}$$

$$\frac{\pi}{6} d^3 \rho_p \frac{d\overrightarrow{\Omega_p}}{dt} = \sum_{i=0}^{N_c} \overrightarrow{T_{C,i}}. \tag{2}$$

In Eq. (1), the first term on the right-hand side is the weight of the particle, the second term corresponds to the sum of N_c solid contact forces applied by the neighbors on the particle, and the third term, $\overrightarrow{F_F}$, is the force induced by an external fluid when considering immersed-like granular flows. The contact force between two particles is denoted $\overrightarrow{F_{C,i}} = \overrightarrow{F_N} + \overrightarrow{F_T}$. This force is the sum of the normal and tangential contact forces, respectively, $\overrightarrow{F_N}$ and $\overrightarrow{F_T}$, which are modeled with spring-dashpot and spring-friction models [34]:

$$\overrightarrow{F_N} = -(k_N \|\overrightarrow{\delta_N}\| + \gamma_N \|\dot{\overrightarrow{\delta_N}}\|)\overrightarrow{n}, \quad \text{with } \overrightarrow{n} = \overrightarrow{\delta_N}/\|\overrightarrow{\delta_N}\|$$

$$\overrightarrow{F_T} = \begin{cases} k_T \overrightarrow{\delta_T} \frac{\|\overrightarrow{F_N}\|\mu_p}{\|k_T \overrightarrow{\delta_T}\|} & \text{if } \|k_T \overrightarrow{\delta_T}\| > \|\overrightarrow{F_N}\|\mu_p, \\ k_T \overrightarrow{\delta_T} & \text{otherwise,} \end{cases} \tag{3}$$

where μ_p is the interparticle friction coefficient, k_N is the normal stiffness, $\overrightarrow{\delta_N}$ and $\overrightarrow{\delta_T}$ are the normal and tangential strains, and γ_N is the normal viscous dissipation obtained from k_N and the normal restitution coefficient e_N [34]. The value of k_N is chosen to respect the rigid grain limit: $k_N = \kappa P_{\max} d$, with κ being the relative dimensionless stiffness $\kappa > 10^4$ [35]. In particular, this latter criterion prevents elasto-platic deformations close to the flow-arrest transition [36]. A sensitivity analysis was performed on κ in the dry frictionless case (see Appendix D). The maximum granular pressure a grain will experience in the system, $P_{\max}$, is calculated considering a grain that is under the pressure of the whole grain layer: $P_{\max} = \rho_p \phi_{\max} h g$. The restitution coefficient is fixed at $e_N = 0.9$, as classically used for glass beads. The tangential stiffness is related to the normal stiffness as $k_T = \nu k_n$, with Poisson's coefficient set to a typical value of $\nu = 0.5$ [36].

In Eq. (2), the term on the right-hand side is the sum of the N_c contact torques. For each contact, the torque is defined as follows: $\overrightarrow{T_C, i} = d(-\overrightarrow{n}) \times (\overrightarrow{F_C, i})$.

When immersed in a fluid at rest, a particle is also subjected to fluid forces [see Eq. (1)]. In the present work, the idea is to model the influence of the fluid on particle behavior at first order. As such, the fluid is considered to be at rest, and we focus on the main fluid forces, which are drag and buoyancy, $\overrightarrow{F_F} = \overrightarrow{F_D} + \overrightarrow{F_B}$. In the Stokes limit, one expects lubrication to appear and play a role in the close contact behavior. Considering that the viscous drag and the lubrication force have the same viscous scaling, the lubrication force is discarded here for the sake of modeling simplicity. This assumption is supported by the low influence of the restitution coefficient observed on the results (see Appendix D). The drag force $\overrightarrow{F_D}$ is classically written as:

$$\overrightarrow{F_D} = -\frac{1}{2}\rho_f \frac{\pi d^2}{4} C_D \| \overrightarrow{u} \| \overrightarrow{u}, \tag{4}$$

with the fluid density ρ_f and where the drag coefficient C_D is modeled to consider both Newton and Stokes regimes [37,38]:

$$C_D = \left(0.44 + \frac{24}{Re_p}\right). \tag{5}$$

The particle Reynolds number, Re_p, is calculated as follows:

$$Re_p = \frac{\rho_f \| \overrightarrow{u} \| d}{\eta_f}, \tag{6}$$

with η_f being the dynamic viscosity of the fluid. The buoyancy force is defined as follows:

$$\overrightarrow{F_B} = -\frac{\pi}{6} d^3 \rho_f \overrightarrow{g}. \tag{7}$$

Considering the equation of motion of a grain between two contacts in the granular system [Eq. (1)] without the contact forces, the dimensionless numbers that drive the behavior of the system are the Stokes number St and the density ratio r [16,20]:

$$St = \frac{\sqrt{\rho_p(\rho_p - \rho_f) g d^3}}{18\eta_f}, \tag{8}$$

$$r = \frac{\rho_p}{\rho_f}. \tag{9}$$

The Stokes number, St, measures the ratio between the inertia of grains versus the viscous dissipation of the fluid. At high Stokes numbers, grain inertia is dominant, equivalent to the dry case ($St = \infty$ numerically), while at low Stokes numbers, the grain dynamics is strongly affected by viscous dissipation in the so-called viscous regime.

The density ratio, r, compares the effect of the buoyancy and the weight of grains and is chosen at $r = 1000$ to get rid of the buoyancy effect and study specifically the effect of viscous dissipation on hysteresis.

The code has been validated, in both the dry and immersed cases, comparing the results in terms of granular velocity and volume fraction profiles [39] and mean granular velocity for different layer thicknesses and Stokes numbers [40].

C. Protocol

Flow arrest and avalanche onset are studied by varying the inclination angle θ of the inclined plane with respect to gravity at a fixed inclination velocity $\delta\theta/\delta t = 10^{-4\circ}/\sqrt{d/g}$, $\delta\theta$ being the angle step and δt the duration between two angle variations. The value of the plane variation velocity was selected by performing a sensitivity analysis similar to that for the domain size (see Supplemental Materials [32]). The slope evolution is quasistatic in the simulations performed and one can consider the granular flow to be steady and uniform in the streamwise and spanwise directions. Under these conditions, the main feature of the inclined plane is that it acts like a rheometer, with the inclination angle imposing the stress state of the granular medium through the shear-to-normal stress ratio

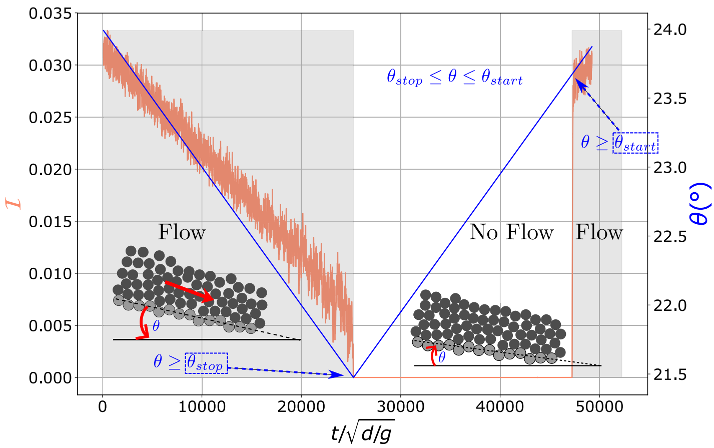

FIG. 2. Inertial number $\mathcal{I}$ (left) and inclination angle θ (right) as functions of time within a simulation.

$\mu = \tau/P$. In the framework of the $\mu(I)$ rheology [3], the latter is a direct function of the dimensionless shear rate, I, so that varying the slope allows one to explore the different granular flow regimes. Moreover, as the average flow only varies along the wall-normal direction, momentum balance along the inclined plane simply leads to the shear-to-normal ratio stress relation $\mu = \tau/P = \tan(\theta)$. Finally, the depth average inertial number I is written as:

$$\mathcal{I} = \frac{1}{h}\int_0^h I(z)\,dz, \tag{10}$$

with $I(z) = d\dot{\gamma}(z)/\sqrt{P(z)/\rho_p}$, which can be directly determined from the vertical velocity profile $\dot{\gamma}(z) = \partial u_x(z)/\partial z$ and the vertical pressure profile $P(z) = \rho_p g\cos(\theta)\int_z^h \phi(z)\,dz$ that depends on the volume fraction profile $\phi(z)$.

Figure 2 shows the inertial number and the plane inclination angle as functions of the time within a simulation to present the protocol used for the simulation performed. The angle of the plane is first set at a high enough angle to set the granular layer in motion associated with a finite value of inertial number. Then the plane inclination angle is continuously decreased at angular velocity $-\delta\theta/\delta t$, as shown by Fig. 2, leading to a decrease of the inertial number, $\mathcal{I}$, until the media stops flowing and the inertial number suddenly drops to zero. In the protocol, the granular medium is considered at rest when the kinetic energy per particle is less than $E_{k,\mathrm{crit}} = 10^{-8}mgd$, which has been checked to correspond to a granular medium at rest. At that time, the granular medium has reached the static state, the stopping angle, θ_{stop}, also called the jamming angle, is measured. The plane angle is then increased with the same angular velocity $\delta\theta/\delta t$ until the medium flows again when the inertial number suddenly and significantly increases as observed in Fig. 2. At that point, the medium starts to flow, and the avalanche angle, θ_{start}, also called the starting angle, is measured.

In this paper, a systematic study is performed on the interparticle friction coefficient, μ_p, and particle inertia. The latter is varied by varying the Stokes number, St, through the fluid viscosity η_f. Each simulation at a given pair of imposed parameters (μ_p, St) is repeated 10 times with randomly generated plane roughness. The results presented in the present paper represent more than 270 simulations corresponding to more than 600 000CPU hours. The calculation time for simulations depends on the number of particles as well as the velocity of angle variation. The latter parameter has been adapted within simulations of immersed media at low Stokes numbers to keep the time between two angle variations, $\delta t/\sqrt{d/g} = 1$, lower than the relaxation time τ_r of a grain in the fluid. This issue occurs for low Stokes numbers and increases drastically the computational time for each

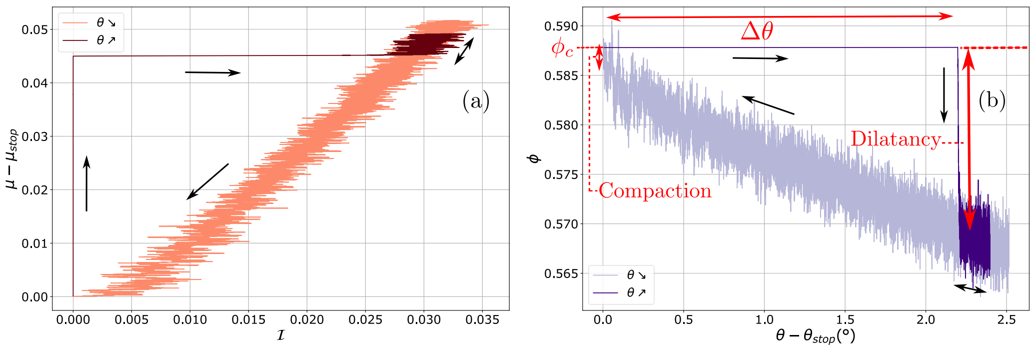

FIG. 3. (a) Hysteretic loop of the relative shear-to-normal stress ratio $\mu(I) - \mu_{\text{stop}}$ as a function of the inertial number, $\mathcal{I}$, for interparticle friction $\mu_p = 0.5$ leading to $\mu_{\text{stop}} = 0.39$. (b) Hysteretic loop of the solid fraction ϕ as a function of the relative inclination angle $\theta - \theta_{\text{stop}}$ for interparticle friction $\mu_p = 0.5$ leading to $\theta_{\text{stop}} = 21.47^\circ$. The arrows, color, and legend indicate for each plot the stress path within hysteretic cycles.

simulation, as the relaxation time is linear with Stokes number variation in the regime explored, $\tau_r = \rho_p d^2/18\eta_f$ (Stokes regime, high-density ratio) [16].

III. COMBINED INFLUENCE OF FRICTION AND INERTIA

Simulations are performed following the protocol defined in Sec. II C and displayed in Fig. 2. Starting from a flowing state, the angle of the inclined plane is progressively decreased down to the cessation of the flow, before ramping up the inclination angle until the flow starts. Measuring the mean inertial number associated with the granular flow, it is possible to observe the hysteretic loop in the context of the $\mu(I)$ rheology [Fig. 3(a)]. In this framework, the granular rheology can be described in terms of the shear-to-normal stress ratio, $\mu = \tau/P$, which is a unique function of the inertial number [3,41], $\mu(I)$. For a steady, uniform inclined plane configuration, the shear-to-normal stress ratio is directly set by the inclination angle of the plane, $\mu = \tan(\theta)$ [2].

Figure 3(a) shows a typical hysteretic loop on $\mu(\mathcal{I})$ that demonstrates the presence of a hysteresis at the transition. Decreasing the inclination angle, the corresponding inertial number decreases and eventually drops to zero at stopping angle $\mu = \mu_{\text{stop}} = \tan(\theta_{\text{stop}})$. The stress path is then reversed and the inclination angle is progressively increased. The granular medium remains static up to the avalanche angle, where the flow comes back to the initial $\mu(I)$ branch. The difference between the avalanche and stopping angle characterizes the hysteresis, $\Delta\mu = \mu_{\text{start}} - \mu_{\text{stop}} = \tan(\theta_{\text{start}}) - \tan(\theta_{\text{stop}})$. For the sake of simplicity and for a more intuitive view of the results, the data are plotted in the following in terms of inclination angle.

It is classical to consider the solid volume fraction variation close to the fluid-to-solid transition [30,42]. It is interesting to note that it is equivalent to considering the $\mu(I)$ rheology in terms of solid volume fraction $\mu(\phi)$, as done in the literature [43]. Figure 3(b) shows the hysteretic loop observed for the volume fraction. As the inclination angle decreases, the granular flow becomes denser, up to the critical solid volume fraction at which the medium comes to rest. Reversing the loading, the solid volume fraction stays constant up to the onset of motion at a larger inclination angle. While the solid volume fraction displays a gap at the initiation of the flow, a signature of dilatancy, it does not seem to exhibit a gap when coming to rest for the present dry configuration with classical interparticle friction coefficient ($\mu_p = 0.5$).

In the following, the results are analyzed quantitatively in terms of critical angles and hysteresis amplitude, $\Delta\theta$, as a function of the grains' inertia (St) and interparticle friction coefficient (μ_p). Each simulation corresponding to a set of parameters (μ_p, St) is repeated 10 times with newly generated bottom roughness to assess the geometrical variability due to the boundary from one

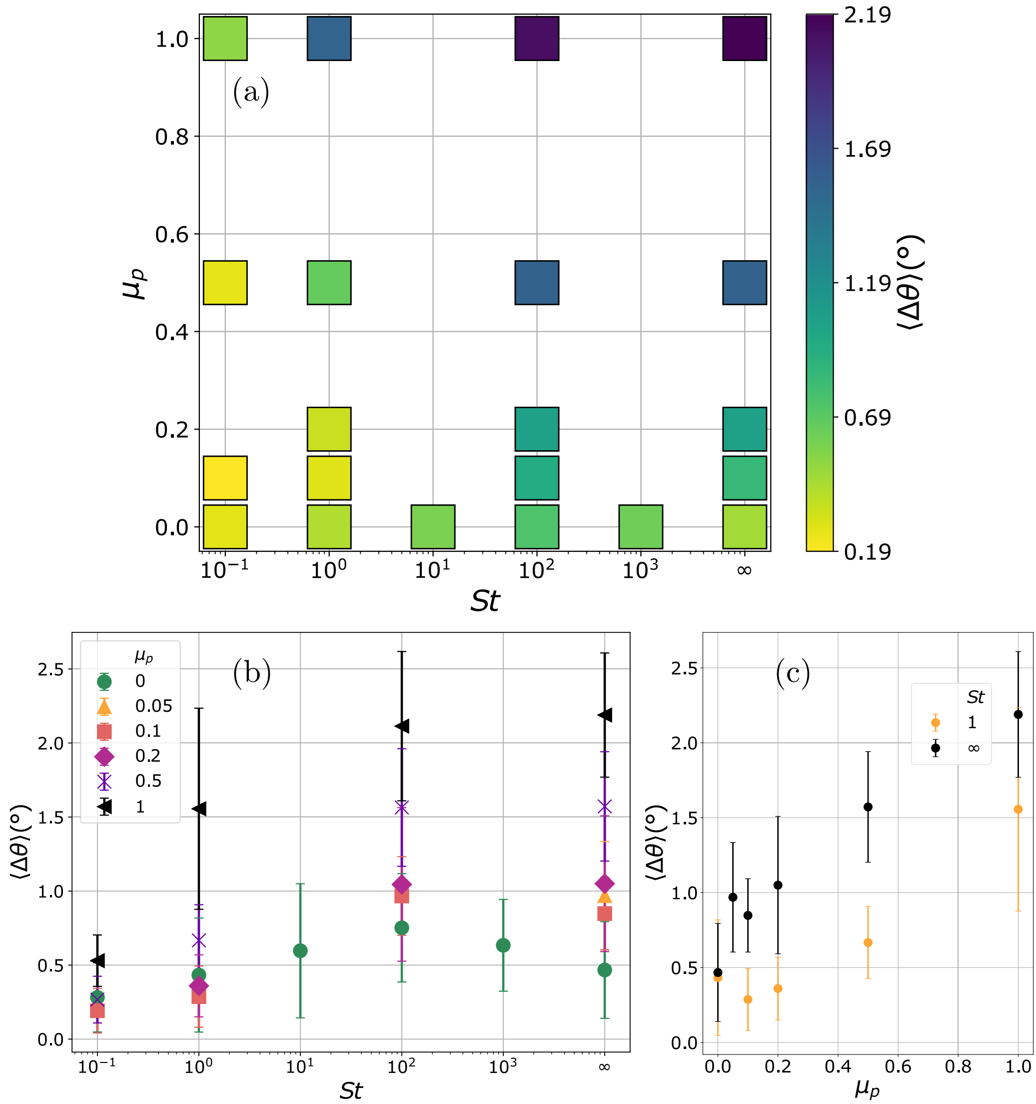

FIG. 4. (a) Hysteresis amplitude as a function of the Stokes number and the microscopic friction coefficient. (b) Evolution of the hysteresis amplitude $\Delta\theta$ with Stokes number at various interparticle friction coefficients. (c) Evolution of the hysteresis amplitude as a function of interparticle friction coefficient μ_p at low Stokes, $St = 1$, and in the dry case, $St = \infty$.

case to another. We expect this variability to be more important than the intrinsic variability of the system due to the stochastic nature of the transition [44]. The data are plotted in terms of averaged parameters, $\langle\cdot\rangle$, and the error bars are characteristic of the geometrical variability and represent the standard deviation observed between the 10 different runs performed for each set of parameters.

Figure 4(a) presents the global picture of the variation of hysteresis amplitude with interparticle friction and Stokes number. It shows that the hysteresis varies globally with both parameters defining different regions in the parameter space: the hysteresis is minimum at low Stokes and low interparticle friction, while it is maximum for dry highly frictional particles. Overall, it tends to decrease with decreasing Stokes number at a given interparticle friction coefficient and to decrease when decreasing interparticle friction coefficient at a given Stokes number.

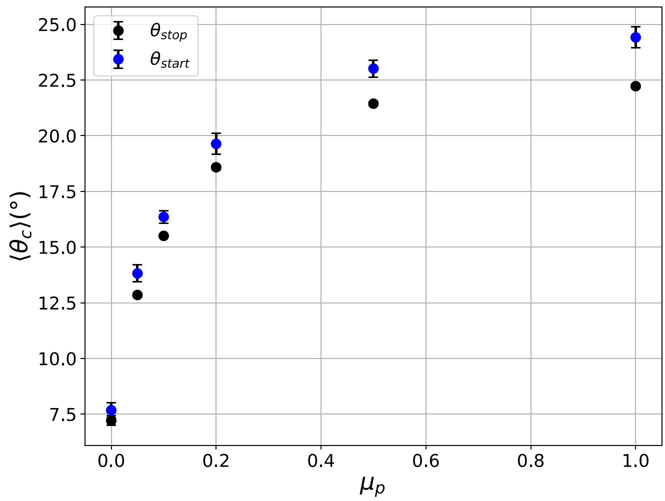

FIG. 5. Evolution of the stop and avalanche angles, θ_{stop} and θ_{start}, with the microscopic friction coefficient in the dry case.

Going into more detail, the results are presented in terms of hysteresis amplitude as a function of the Stokes number for various microscopic friction in Fig. 4(b). They are also presented in Fig. 4(c) as a function of the friction coefficient for Stokes number one, $St = 1$, and in the dry case, $St = \infty$. It can be observed that (i) the average hysteresis amplitude, $\langle \Delta\theta \rangle$, is an increasing function of the interparticle friction μ_p at all Stokes numbers. It is approximately divided by four between $\mu_p = 1$ and frictionless particles; (ii) the hysteresis amplitude decreases with the Stokes number for low $St < 100$ and remains nearly constant for $St \geqslant 100$ for all μ_p, the results obtained are consistent with the experimental data from the literature, as detailed in Appendix A; (iii) for frictionless particles, the hysteresis amplitude is finite in the dry configuration, and tends toward zero with decreasing Stokes number.

These results show a dominant effect of microscopic friction on hysteresis amplitude, consistent with the literature [19–21]. Meanwhile, the influence of the Stokes number on the results shows that there is a non-negligible effect of the fluid viscous dissipation on hysteresis amplitude, in agreement with Courrech Du Pont *et al.* [16] (see Appendix A). This shows that hysteresis is also influenced by grains' inertia, and suggests that it is necessary to have both frictionless particles and low Stokes number to cancel hysteresis. Therefore, the present results suggest that if Perrin *et al.* [20,31] observed an absence of hysteresis for frictionless particles, it is probably because they are considering overdamped experiments with very low Stokes numbers.

As presented here, hysteresis is classically expressed in terms of its absolute value. The amplitude of hysteresis defines the region where the possible stability of a granular medium depends on the stress path. As such, it seems relevant to compare the amplitude of hysteresis with respect to the angles of stability of the granular medium. Indeed, the latter are varying importantly with interparticle friction coefficient, as shown by Fig. 5. Accordingly, Fig. 6(a) presents the hysteresis amplitude normalized by the avalanche angle for all the data, with the variation of both Stokes number and interparticle friction coefficient. The results show that the relative hysteresis is of the same order of magnitude for all the simulations (2% to 10%). Figure 6(b) evidences further that, while hysteresis amplitude appears lower for frictionless particles [Fig. 4(c)], its relative importance with respect to stability is similar to that observed for finite interparticle friction coefficients. Also, one can observe more clearly the nontrivial combined effect of interparticle friction and Stokes number. Figure 6(a) shows a decreasing trend of the relative hysteresis with decreasing Stokes number at finite interparticle friction coefficient. In addition, the figure shows that the relative amplitude of hysteresis is lower for intermediate interparticle friction than for frictionless and highly

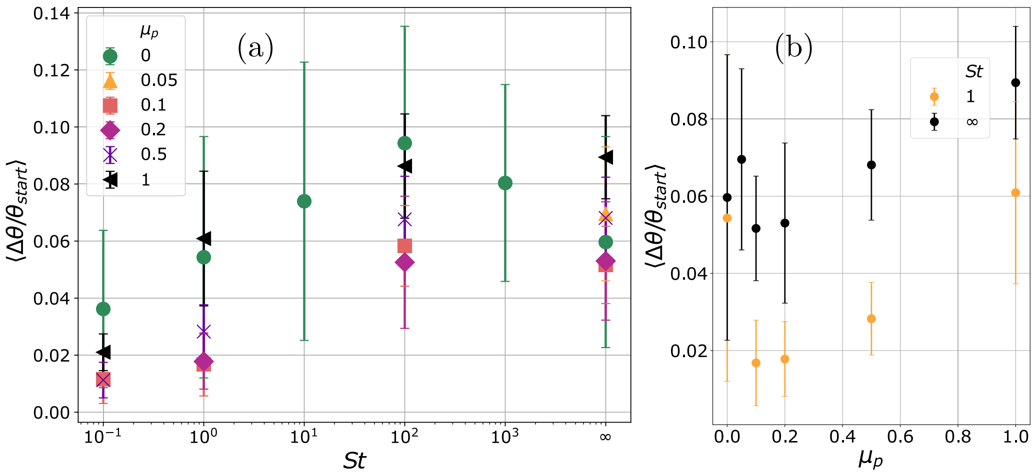

FIG. 6. (a) Hysteresis amplitude relative to the avalanche angle $\Delta\theta/\theta_{\mathrm{start}}$ as a function of the Stokes number for various microscopic friction coefficients. (b) Hysteresis amplitude relative to the avalanche angle $\Delta\theta/\theta_{\mathrm{start}}$ versus microscopic friction coefficient μ_p at low Stokes, $St = 1$, and in the dry case, $St = \infty$.

frictional particles. It is well highlighted when plotting the relative hysteresis versus the friction coefficient for low Stokes number, $St = 1$, and in the dry case, $St = \infty$, as shown by Fig. 6(b). This nontrivial combined influence of microscopic friction and grains' inertia might be related to changes in the main local particle behavior, which can shift from rolling to sliding as a function of the parameters. This difference in local behavior has been shown to lead similarly to differences in global behavior for dry granular flows [22].

Finally, it is important to underline that the different results presented exhibit a finite hysteresis in the frictionless dry particle case ($\mu_p = 0$, $St = \infty$). We have shown that this observation is independent of the domain size, layer thickness, restitution coefficient, and velocity of angle variation (see Appendices B, C, and D), and the discontinuity of the transition is even increasing with increasing particle stiffness (see Appendix D). This analysis of the sensitivity to model and physical parameters demonstrates the robustness of the presence of a finite hysteresis for frictionless particles in the dry case. This result is incompatible with the framework of DeGiuli and Wyart [21], in which interparticle friction is necessary to observe hysteresis.

To conclude, the present results show that hysteresis is linked to both particle friction and inertia, rationalizing the different results from the literature highlighting hysteresis dependency on either friction [19,20] or inertia [16], and suggesting the need for further improvement of the established framework. In addition, the presence of hysteresis for frictionless particles seems in apparent contradiction with the vanishing dilatancy observed in such cases [42]. The absence of dilatancy at the transition suggested a continuous second-order jamming transition [45] and, accordingly, the absence of hysteresis for frictionless particles [20,31,46].

IV. HYSTERESIS AND DISCONTINUITY OF THE TRANSITION: THE ROLE OF MICROSTRUCTURE DESCRIPTORS

A. Hysteretic cycles of the solid volume fraction and coordination number for frictionless materials

The singularity of the frictionless case, as well as the finite hysteresis value observed, leads us to analyze how the transition can be discontinuous for frictionless materials and, specifically, how this discontinuity can be characterized.

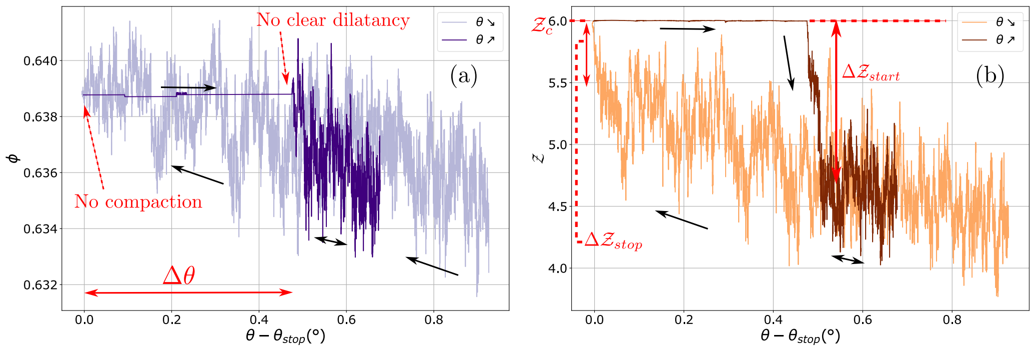

FIG. 7. Hysteretic loop of the volume fraction ϕ (a) and coordination number $\mathcal{Z}$ (b) versus the relative inclination angle, $\theta - \theta_{\text{stop}}$, with frictionless particles ($\mu_p = 0$). The stopping angle is $\theta_{\text{stop}} = 7.09°$. The black arrows, curve colors, and legend indicate for each plot the stress path within hysteretic cycles. Characteristic values of ϕ and $\mathcal{Z}$ are also illustrated in the plots.

To do so, the hysteretic loop of the solid volume fraction and the coordination number in the dry frictionless case ($\mu_p = 0$, $St = \infty$) are studied. Figure 7(a) shows the hysteretic cycle for the solid volume fraction $\phi(\theta)$. This figure shows that frictionless grains exhibit a hysteresis at the transition. While the importance of the gap observed in terms of inclination angle, $\Delta\theta$, is lowered with respect to the frictional case [see Fig. 3(b)], the presence of a discontinuity is clear for the system considered. Interestingly, the solid volume fraction appears to evolve continuously toward jamming, as it increases and oscillates around the solid volume fraction at rest before jamming. Similarly, no clear dilatancy is observed when the medium is set into motion while increasing the inclination angle. This absence of apparent compaction and dilatancy on the volume fraction, respectively, at jamming and unjamming, which were both present in the frictional case at $\mu_p = 0.5$, albeit weakly for the first one, must be interpreted as the fact that the volume fraction evolves continuously into the random close packing at the flowing-to-static transition and similarly at the static-to-flowing transition. This result is consistent with the observation that frictionless granular media exhibit no dilatancy [42,47].

The results observed show that the apparent continuity of behavior in terms of solid volume fraction is not associated with the absence of hysteresis. The solid volume fraction is therefore not the relevant proxy to characterize the hysteresis associated with the transition.

To characterize the microstructure of the granular material from a different perspective, we consider the coordination number of the system, that is, the average number of contacts per grain $\mathcal{Z}$. The calculation of the coordination number is detailed in Appendix E. This approach allows us to obtain the isostatic limit of the coordination number for frictionless granular media at rest, $\mathcal{Z}_c = 6$, as shown in Fig. 7(b). Similar to the solid volume fraction, this critical value of the coordination number in the static state is constant with variations of stress and displays tiny variations that are the signature of local rearrangement in the system. The critical value of the coordination number is consistent with the theoretical prediction using Maxwell's mechanical equilibrium criterion that gives for frictionless spherical particles $\mathcal{Z} = 6$ [8,48–50]. In addition, the coordination number increases with the decrease in the angle in the flowing regime. This behavior is equivalent to the increase in the flowing volume fraction with decreasing inclination angle but at the microstructure scale. The denser the medium, the more particles are in contact. Yet, unlike volume fraction, the coordination number displays a discontinuity at both the cessation of flow, noted $\Delta\mathcal{Z}_{\text{stop}}$, and the initiation of flow, noted $\Delta\mathcal{Z}_{\text{start}}$. These discontinuities in the coordination number value are clear and increase with increasing particle stiffness (see Appendix D), highlighting the presence of hysteresis at the transition. These discontinuities are a signature that the contact network compacts and dilates, respectively, at jamming and unjamming

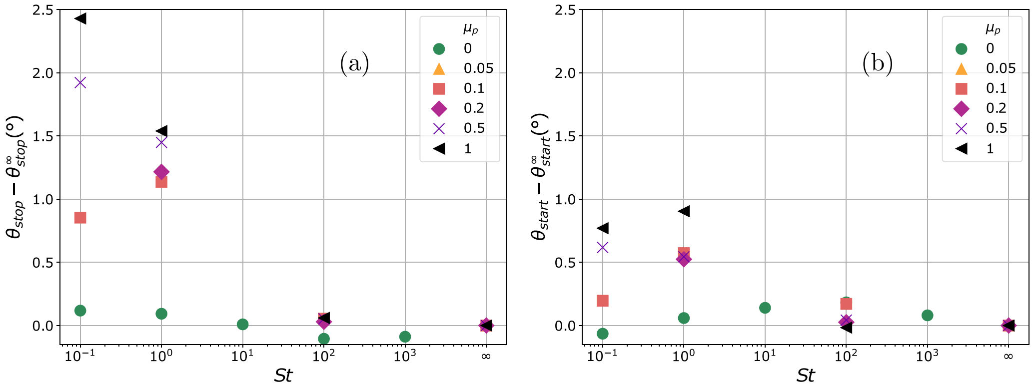

FIG. 8. (a) Difference between the stop angle in the immersed cases and the stop angle in the dry case $\theta_{\text{stop}} - \theta_{\text{stop}}^{\infty}$, $\theta_{\text{stop}}^{\infty} = \theta_{\text{stop}}(St = \infty)$, versus the Stokes number at various friction coefficients. (b) Difference between the start angle in the immersed cases and the start angle in the dry case $\theta_{\text{start}} - \theta_{\text{start}}^{\infty}$, $\theta_{\text{start}}^{\infty} = \theta_{\text{start}}(St = \infty)$, versus the Stokes number at various friction coefficients.

transitions and capture the fact that the flow-arrest transition remains hysteretic in the dry frictionless case.

B. Toward a description of the influence of the microstructure on hysteresis

To better characterize and understand the physical mechanisms behind the observed hysteresis, it is interesting to discuss the results observed in terms of stopping and starting angles.

Figure 5 shows the important variation in the avalanche (θ_{start}) and stopping (θ_{stop}) angles with interparticle friction. These important variations do not allow one to observe well the impact of a given parameter on hysteresis. Indeed, fine variations in the avalanche or stopping angle with respect to its absolute value lead to important impacts on hysteresis. Therefore, to characterize the influence of the Stokes number on the avalanche and stopping angles and their impacts on hysteresis, we consider the difference between the avalanche (stopping) angle at the given Stokes number and the avalanche (stopping) angle in the dry case [see Figs. 8(a) and 8(b)]. The evolution observed for both angles is not monotonous and presents the most important relative variations for Stokes number one. The variations are approximately twice higher on the stopping angle than on the avalanche angle. In this case, the fluid viscous dissipation has the effect of increasing the stopping angle toward the avalanche angle, leading to lower hysteresis when Stokes tends toward zero, as presented in Sec. III.

Beyond the role of inertia and friction, one may attempt to characterize the avalanche angle, stopping angle, and hysteresis in terms of the coordination number characterizing the granular microstructure, as discussed in the previous section. Figure 9(a) presents the avalanche angle as a function of the coordination number at rest. The latter evolves as expected between $\mathcal{Z}_c(\mu_p \to \infty) = 4$ and the higher bound in the frictionless case $\mathcal{Z}_c(\mu_p = 0) = 6$ [50,51] (see Appendix E for further details on the stable state characterization). The variation of the avalanche angle with particle friction and inertia appears to be directly related to the variation of the coordination number at rest. For moderate and high interparticle friction coefficients, the variation of the avalanche angle with the Stokes number observed in Fig. 9 is, in fact, due to the change in coordination number in the static state. As such, it appears as a consequence of the modification of the jamming angle due to the influence of the surrounding fluid. The fact that the avalanche angle depends solely on the static coordination number is a consequence of the arrangement of the granular medium at rest. Meanwhile, the loading process from the static state has been observed to be a dynamic process in the literature [24,26,27] as well as in the present study [45], with rearrangement occurring continuously with increasing angle before reaching failure. The present result, therefore, suggests

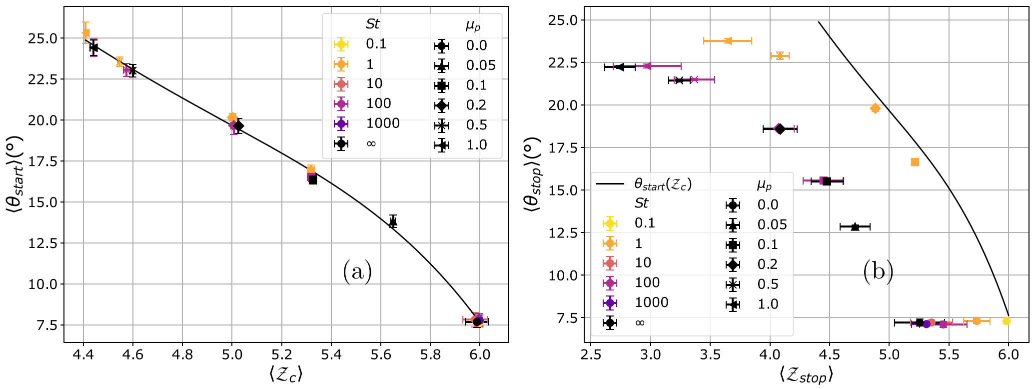

FIG. 9. (a) Evolution of the avalanche angle θ_{start} with the coordination number in the static state, $\mathcal{Z}_c$, at various microscopic friction coefficients and Stokes numbers. (b) Evolution of the stop angle θ_{stop} with the coordination number in the flowing state before jamming, $\mathcal{Z}_{\text{stop}}$, at various microscopic friction coefficients and Stokes numbers. The solid line is a fit for the eye of the avalanche angle as a function of the static coordination number with a degree-4 polynomial function. It is reproduced in (b) to consider the evolution of the difference between the avalanche and the stop angle (i.e., the hysteresis amplitude) as a function of the parameters.

that the onset of motion linked to progressive rearrangement is weakly influenced by the presence of an interstitial fluid.

Jamming occurs with complex dissipation processes in the flowing state since it results from the self-sustainability of perturbations. Characterizing the stopping angle with microstructure state variables is then more complex than with the avalanche angle, and no microstructure variable equivalently captures viscous and friction dissipation influences on the stopping angle. Meanwhile, it is possible to understand the mechanisms at play by considering the evolution of the coordination number in the flowing state before jamming, $\mathcal{Z}_{\text{stop}}$. The latter is measured by fitting the trend of the coordination number evolution before jamming and extrapolating the results at $\theta = \theta_{\text{stop}}$. Figure 9(b) presents the evolution of the stopping angle as a function of this variable. The black curve is the fit of the starting angle dependence on the coordination number in the static state $\theta_{\text{start}}(\mathcal{Z}_c)$. For a given Stokes number, the stopping angle is observed to be a decreasing function of the coordination number in the flowing state before jamming, similar to the trend observed for the avalanche angle with the critical coordination number. When lowering the Stokes number at a given friction coefficient, $\mathcal{Z}_{\text{stop}}$, tends toward the static coordination number so that the discontinuous jump at jamming tends toward zero. This suggests that the stopping goes toward the avalanche angle, and hysteresis amplitude decreases.

Accordingly, Fig. 10 presents hysteresis amplitude as a function of the discontinuity of the coordination number at the jamming transition, defined as $\Delta\mathcal{Z}_{\text{stop}} = \mathcal{Z}_c - \mathcal{Z}_{\text{stop}}$ the difference between the static coordination number, $\mathcal{Z}_c$, and the coordination number in the flowing state before jamming $\mathcal{Z}_{\text{stop}}$. It can be observed that the hysteresis amplitude scales correctly with this discontinuity, making microscopic friction and viscous dissipation collapse on the same curve $\langle\Delta\theta(\langle\Delta\mathcal{Z}_{\text{stop}}\rangle)\rangle$. The discontinuity measures how much the self-sustainability process leads to higher hysteresis by lowering the number of contacts in the flowing state $\langle\mathcal{Z}_{\text{stop}}\rangle$ compared with the value required to be stable $\langle\mathcal{Z}_c\rangle$. In other words, when independently decreasing the microscopic friction coefficient or the Stokes number, hysteresis amplitude, as much as the discontinuity of coordination number at jamming, are equivalently decreasing. This shows that the hysteresis of the transition between the liquid-like and solid-like behaviors of granular media down the inclined plane can be characterized by the discontinuity of the coordination number at jamming. In particular, the absence of coordination number discontinuity at jamming should be characteristic of an absence of hysteresis. In this case, the transition is expected to be reversible and without hysteresis. Here, it can be observed

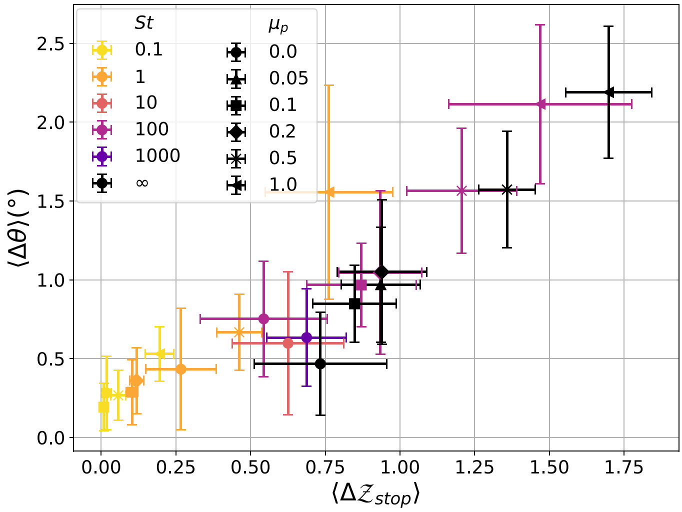

FIG. 10. Hysteresis amplitude $\Delta\theta$ versus the coordination number discontinuity at jamming $\Delta\mathcal{Z}_{\text{stop}}$.

that the hysteresis amplitude is not dropping to zero while the discontinuity of the coordination number is almost vanishing in Fig. 10. The artificially low contact stiffness used in the simulations for computational reasons leads to an underestimation of the discontinuity of coordination number for a given hysteresis as shown in Appendix D (see Fig. 13). This underestimation should shift the points in Fig. 10 to the right, and we expect to recover the right trend accordingly.

V. CONCLUSION

This work presented a numerical analysis of hysteresis on an inclined plane by means of 3D numerical simulations of monodisperse granular media. Modeling the behavior of all the particles, configurations with and without a model surrounding fluid were simulated. A reproducible protocol to study hysteresis was developed and validated. Taking advantage of the numerical facility, an extensive numerical campaign was performed, varying both the interparticle friction coefficient and the Stokes number, accounting for particle inertia.

The results show that the amplitude of hysteresis depends on the combined influence of both particle friction and inertia in the inclined plane configuration. In particular, this amplitude is observed to decrease with decreasing friction, and to decrease with decreasing inertia. This leads to a negligible hysteresis only when both effects, friction and inertia, are canceled out. The present results and analysis then allow us to rationalize the different existing results on hysteresis amplitude dependency through either friction or inertia. This contrasts with the framework proposed by DeGiuli and Wyart [21], predicting no hysteresis in the absence of interparticle friction, and therefore suggests the need for further development to account for inertia effects.

The present work also shows that hysteresis can be present even when the solid volume fraction does not display discontinuities at the jamming and unjamming transitions. Yet, the coordination number characterizes well the transition discontinuity, and hysteresis amplitude has been shown to scale with the coordination number discontinuity at jamming. These results highlight the strong link between the jamming-unjamming transition and the evolution of the granular microstructure through friction and inertia.

Further work is required to model hysteresis as a function of microstructure descriptors and implement such description in a continuous rheological model accounting for the hysteresis at the static-flowing transition, such as in Edwards *et al.* [11]. In particular, the present work was done considering inclined plane simulations. The comparison with the literature, as well as the possible interplays between hysteresis and finite-size effects [12,31], suggest an interest in performing similar analyses in different configurations.

ACKNOWLEDGMENTS

The authors thank Chris G. Johnson and Franco Tapia for discussions about the nature of hysteresis and granular rheology. This research was supported by the French Ministry of Research and Education. The authors were granted access to the HPC resources of the CALMIP supercomputing center under the allocations 2022-p21051, 2023-p21051, and 2024-p21051.

APPENDIX A: COMPARISON WITH THE LITERATURE: THE INFLUENCE OF STOKES NUMBER ON HYSTERESIS

The simulation results presented in this paper in terms of hysteresis as a function of the Stokes number are compared with the results in the literature in Fig. 11. The main experimental results from the literature on the influence of Stokes number have been made in rotating drums [16,20], and are therefore completed with experimental data from an inclined plane configuration [3]. The result observed in the present paper for a dry configuration ($St = \infty$ in Fig. 11) with moderate interparticle friction coefficient ($\mu_p = 0.5$) shows a similar hysteresis amplitude as the one observed experimentally in the same configuration by Forterre and Pouliquen [3]. This hysteresis observed on an inclined plane is slightly lower than the one observed in rotating drums [16], suggesting an influence of the configuration geometry on the phenomenon. Besides, Fig. 11 shows that the trend observed experimentally in the literature with varying Stokes numbers is recovered in our simulations. In particular, the simulation results at high interparticle friction coefficient $\mu_p = 1$ lie within the experimental data over the whole range of Stokes numbers studied ($St \in [10^{-1}, 10^4]$). This tends to confirm the relevance of the simulations performed and the results obtained.

APPENDIX B: VELOCITY OF ANGLE VARIATION EFFECT IN THE FRICTIONLESS CASE

The velocity of angle variation is a parameter that could play a role in hysteresis since a lower value implies an increase in the probability of exploring stable configurations while the medium

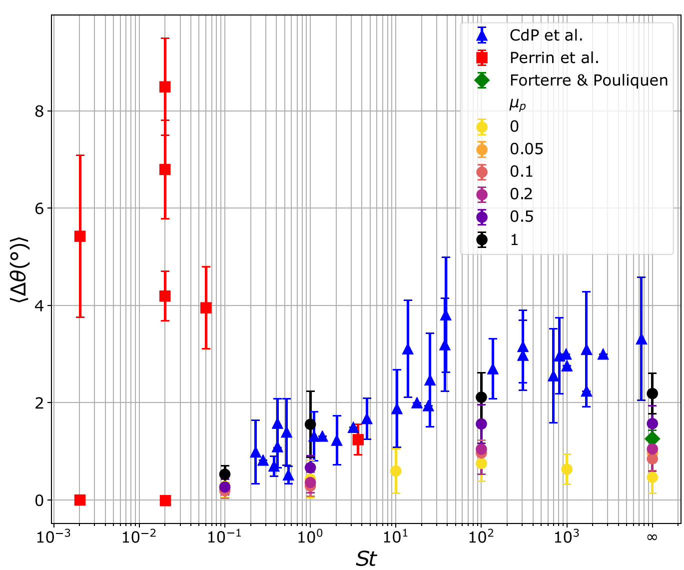

FIG. 11. Hysteresis $\Delta\theta$ versus Stokes number: comparison with the results from the literature in a rotating drum [16,20] and on an inclined plane [3].

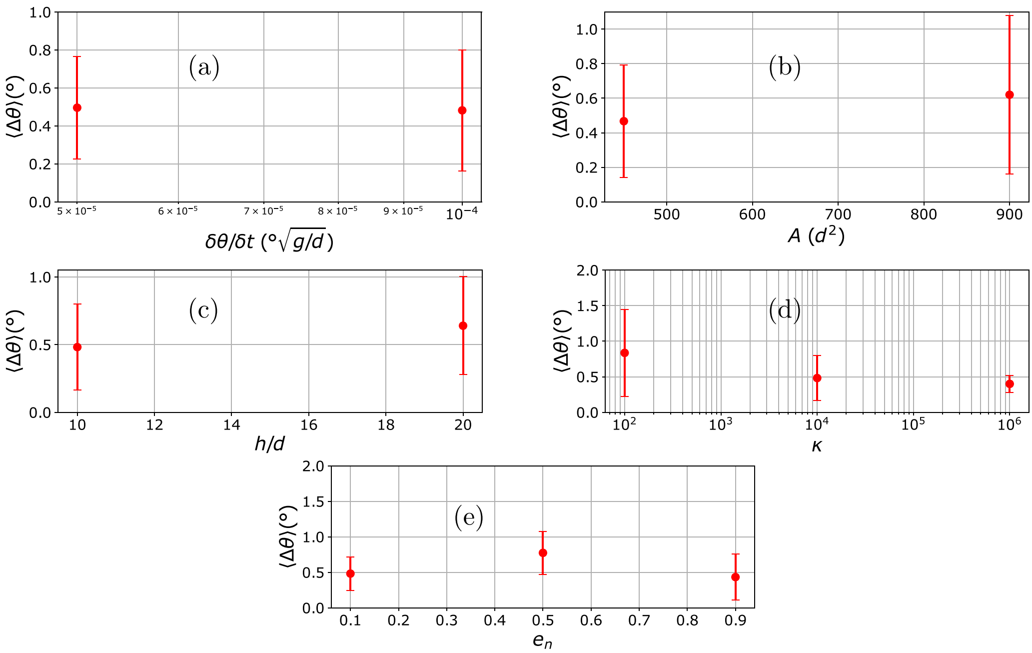

FIG. 12. Evolution of hysteresis $\Delta\theta$ with the velocity of angle imposition (a), the size of the domain $A = L \times W$ (b), the thickness of the grain layer h (c), the dimensionless stiffness κ (d) and the restitution coefficient e_n (e) in the dry frictionless case ($\mu_p = 0$, $St = \infty$).

flows near the jamming conditions. To test the sensitivity of hysteresis to this parameter in the dry frictionless case, simulations have been performed for slower velocity of stress imposition $\delta\theta/\delta t$ than in the reference case of the paper, $\delta\theta/\delta t = 10^{-4\circ}\sqrt{g/d}$. The results are presented in Fig. 12(a). This figure shows that the hysteresis is indeed constant and is not dependent on this parameter in the frictionless case.

APPENDIX C: SIZE EFFECT IN THE FRICTIONLESS CASE

Similarly, size effects could be responsible for the finite hysteresis measured in the frictionless dry case. Indeed, the curves $h_{\text{stop}}(\theta)$ and $h_{\text{start}}(\theta)$, or equivalently, $\theta_{\text{stop}}(h)$ and $\theta_{\text{start}}(h)$, are converging for $h \approx 10d$. However, the effect of the distance between the plane and the free surface could be non-negligible for frictionless beads. To test the sensitivity of hysteresis in the dry frictionless case, a bigger layer thickness $h/d = 20$ has been tested [see Fig. 12(c)]. This result shows that, above $h/d = 10$, the amount of hysteresis measured does not depend on the layer thickness. This is consistent with the results of Pouliquen and Forterre [13].

In a similar way, domain size could also be responsible for the amount of hysteresis measured since a bigger domain implies an increase in the probability of exploring stable configurations while the medium flows near the jamming conditions. This could affect the value of the stop angle. It also implies an increase in the probability that a local rearrangement destabilizes the layer while the medium is static, which could lead to variations in the avalanche angle. Then, simulations were computed in the frictionless case for a bigger domain size $A = L \times W$ than the one in the reference case $L \times W = 30d \times 15d$. The result is presented in Fig. 12(b). This figure shows no particular effect of the increase of domain size. See the Supplemental Materials [32] for further study of the sensitivity analysis for domain size effect.

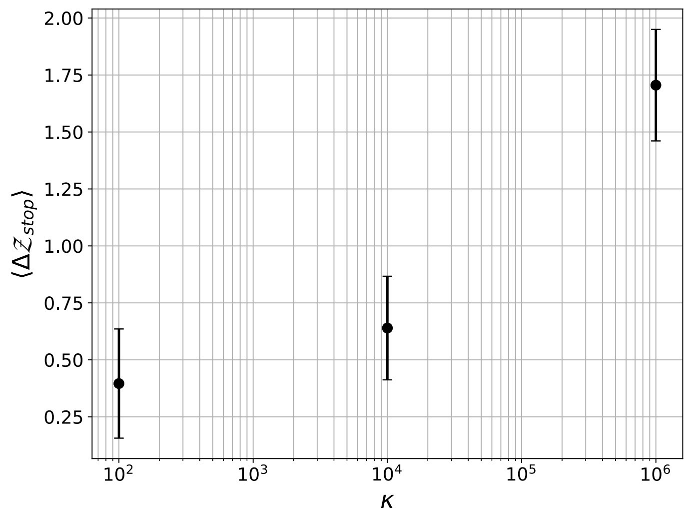

FIG. 13. Coordination number gap at jamming versus relative stiffness in the dry frictionless case ($\mu_p = 0$, $St = \infty$).

APPENDIX D: DIMENSIONLESS STIFFNESS AND RESTITUTION COEFFICIENT EFFECT IN THE FRICTIONLESS CASE

Finally, the stiffness effect on hysteresis has been highlighted by DeGiuli and Wyart [21]. Other studies have shown an effect of stiffness on the stable state [42,48] and in the flowing regime in the quasistatic limit [36,42]. To test the sensitivity of hysteresis with relative stiffness in the dry frictionless case, we computed simulations for different values of the relative stiffness κ. The results are presented in Fig. 12(d). The reference value of relative stiffness in the simulations in this paper is the rigid grain limit defined by Roux and Combe [35] $\kappa = 10^4$. The results show that hysteresis does not vary for relative stiffness higher than the rigid grain limit, validating the choice of this value in the simulations. It also shows that this parameter is not responsible for the amount of hysteresis measured in the frictionless case. In addition, the discontinuity of the coordination number at the jamming transition, $\Delta\mathcal{Z}_{\rm stop}$, is plotted as a function of the relative stiffness in the dry frictionless case ($\mu_p = 0$, $St = \infty$) in Fig. 13. This figure shows that increasing the relative stiffness also increases the discontinuity of the coordination number at the jamming transition.

The normal dissipation of dynamic contacts, that is, at grain collisions, is modeled through the restitution coefficient e_n, which could also eventually play a role in the value of critical angles, hence hysteresis. Simulations have been conducted in the frictionless case for a lower restitution coefficient than the reference one in the simulations $e_n = 0.9$. The results are shown in Fig. 12(e). This figure shows the nontrivial effect of the restitution coefficient, except that it cannot lower the hysteresis value for frictionless particles.

APPENDIX E: COORDINATION NUMBER AND VOLUME FRACTION IN THE STABLE STATE

The coordination number, presented in Sec. IV A, is defined as:

$$\mathcal{Z} = \frac{2N_c^{\rm dyn-dyn} + N_c^{\rm dyn-plane}}{N_p^{\rm dyn}}. \tag{E1}$$

Considered in the calculation are the contacts between two dynamic particles, i.e., particles that are allowed to be in motion in the system, $N_c^{\rm dyn-dyn}$, which is counted twice to account for both particles. On the other hand, a contact between a dynamic particle and a fixed particle, glued at the bottom, that constituted the plane, $N_c^{\rm dyn-plane}$, is only considered once. Figure 14(a) shows the evolution of the

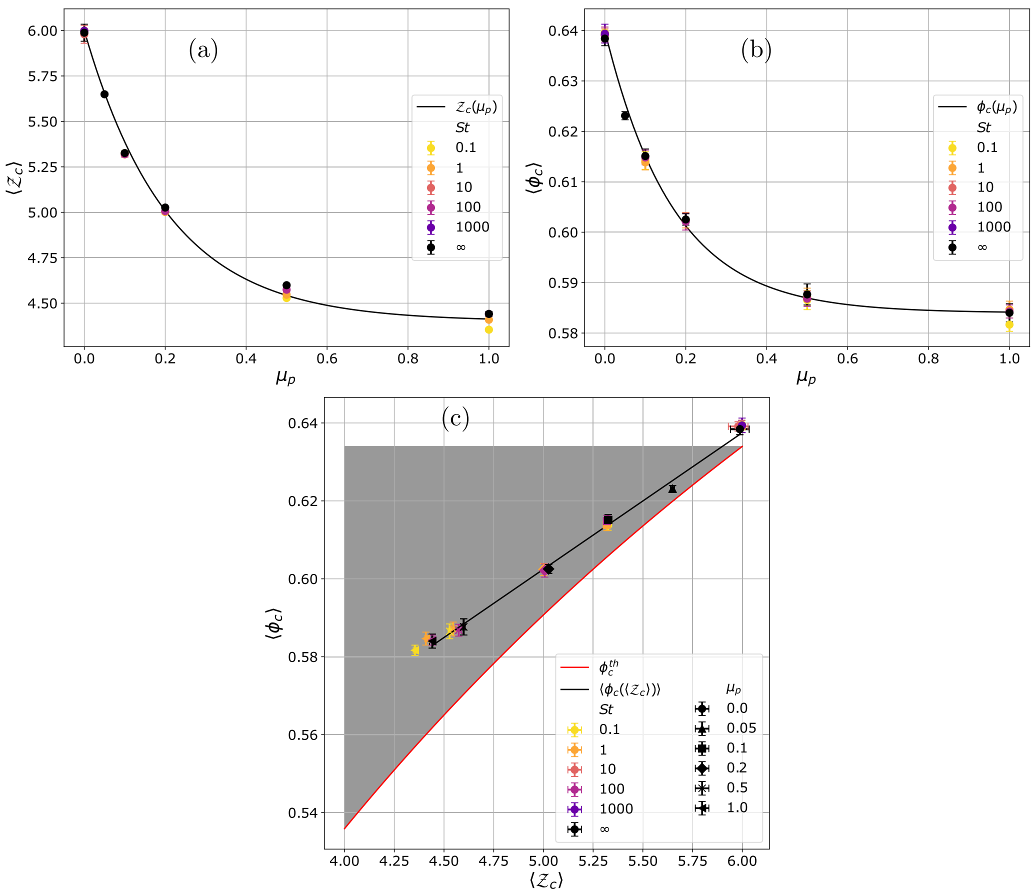

FIG. 14. (a) Evolution of the critical coordination number in the stable state $\mathcal{Z}_c$ with the microscopic friction coefficient at various Stokes numbers. (b) Evolution of the critical volume fraction in the stable state ϕ_c with the microscopic friction coefficient at various Stokes numbers. (c) Critical volume fraction versus coordination number at various microscopic friction coefficients and Stokes numbers. Compared with the phase diagram of jammed matter developed theoretically by Song *et al.* [51].

critical coordination number on the stable state as a function of the microscopic friction coefficient and for various Stokes numbers. It is observed that $\langle \mathcal{Z}_c \rangle$ is in between the lower bound for infinite friction coefficient $\mathcal{Z}_c(\mu_p \to \infty) = 4$ and the higher bound in the frictionless case $\mathcal{Z}_c(\mu_p = 0) = 6$, and varies with microscopic friction coefficient. These bounds and variations of the coordination number in the stable state were extensively studied [48,50,51]. It has been demonstrated that the bounds could be easily calculated by counting the number of constraints and degrees of freedom in the system and calculating the limit values for frictionless particles and infinitely frictional ones with the Maxwell criteria of stability of a mechanical system. This figure shows the dominant effect of the microscopic friction coefficient on the state of the contact network in the stable state. This was highlighted by Silbert *et al.* [48], who also show the effect of the restitution coefficient and the grain stiffness on the contact network density $\mathcal{Z}_c$ and the macrodensity ϕ_c in the stable state. This latter effect on the coordination number has also been highlighted by Favier de Coulomb *et al.* [36].

Interestingly, the variations of the macrodensity, that is, the volume fraction ϕ, with both friction and Stokes number, are presented in Fig. 14(b) and appear to be similar to those of the coordination number. The variations are also dominated by the Coulomb criteria μ_p, which drives the density of the system in the jammed state. The volume fraction is also bounded between the Random

Close Packing, $\phi_{\mathrm{RCP}} = 0.64$ in the frictionless case and the Random Loose Packing, $\phi_{\mathrm{RLP}} = 0.55$ in the high frictional case [51]. This similar evolution of both the coordination and the volume fraction in the jammed state was highlighted by Silbert *et al.* [48]. It appears that the density of the contact network and the density measured at the macroscale are linked in the stable state. This idea was developed in the work of Song *et al.* [51], who defined a phase diagram of jammed granular materials. In the phase diagram plotted in Fig. 14(c), the evolution of the volume fraction is linear with the coordination with the variations of friction in our simulations. Considering that in the frictionless case $\mathcal{Z}_c = 6$ and $\phi_c = \phi_{\mathrm{RCP}}$, and in the limit of infinite friction $\mathcal{Z}_c = 4$ and $\phi_c = \phi_{\mathrm{RLP,min}}$, the following equation between the coordination number and the volume fraction in the stable state in the inclined plane configuration is given:

$$\phi_c = \tfrac{1}{2}(\phi_{\mathrm{RCP}} - \phi_{\mathrm{RLP,min}})\mathcal{Z}_c + (3\phi_{\mathrm{RLP,min}} - 2\phi_{\mathrm{RCP}}). \tag{E2}$$

[1] H. M. Jaeger, S. R. Nagel, and R. P. Behringer, Granular solids, liquids, and gases, Rev. Mod. Phys. **68**, 1259 (1996).

[2] B. Andreotti, Y. Forterre, and O. Pouliquen, *Granular Media: Between Fluid and Solid* (Cambridge University Press, Cambridge, 2013).

[3] Y. Forterre and O. Pouliquen, Flows of dense granular media, Annu. Rev. Fluid Mech. **40**, 1 (2008).

[4] GDR MiDi, On dense granular flows, Eur. Phys. J. E **14**, 341 (2004).

[5] D. J. Jerolmack and K. E. Daniels, Viewing Earth's surface as a soft-matter landscape, Nat. Rev. Phys. **1**, 716 (2019).

[6] P. G. De Gennes, Granular matter: A tentative view, Rev. Mod. Phys. **71**, S374 (1999).

[7] G. Mollon, Mécanique des matériaux granulaires, University Lecture, 2015.

[8] I. Srivastava, L. E. Silbert, J. B. Lechman, and G. S. Grest, Flow and arrest in stressed granular materials, Soft Matter **18**, 735 (2022).

[9] I. S. Aranson, L. S. Tsimring, F. Malloggi, and E. Clément, Nonlocal rheological properties of granular flows near a jamming limit, Phys. Rev. E **78**, 031303 (2008).

[10] R. Artoni, A. Santomaso, and P. Canu, Hysteresis in a hydrodynamic model of dense granular flows, Phys. Rev. E **83**, 051304 (2011).

[11] A. N. Edwards, A. S. Russell, C. G. Johnson, and J. M. N. T. Gray, Frictional hysteresis and particle deposition in granular free-surface flows, J. Fluid Mech. **875**, 1058 (2019).

[12] S. Mowlavi and K. Kamrin, Interplay between hysteresis and nonlocality during onset and arrest of flow in granular materials, Soft Matter **17**, 7359 (2021).

[13] O. Pouliquen and Y. Forterre, Friction law for dense granular flows: Application to the motion of a mass down a rough inclined plane, J. Fluid Mech. **453**, 133 (2002).

[14] A. Daerr and S. Douady, Two types of avalanche behaviour in granular media, Nature (London) **399**, 241 (1999).

[15] F. Da Cruz, F. Chevoir, D. Bonn, and P. Coussot, Viscosity bifurcation in granular materials, foams, and emulsions, Phys. Rev. E **66**, 051305 (2002).

[16] S. Courrech du Pont, P. Gondret, B. Perrin, and M. Rabaud, Granular avalanches in fluids, Phys. Rev. Lett. **90**, 044301 (2003).

[17] L. E. Silbert, D. Ertaş, G. S. Grest, T. C. Halsey, D. Levine, and S. J. Plimpton, Granular flow down an inclined plane: Bagnold scaling and rheology, Phys. Rev. E **64**, 051302 (2001).

[18] O. Pouliquen, Scaling laws in granular flows down rough inclined planes, Phys. Fluids **11**, 542 (1999).

[19] A. Peng, Y. Yuan, and Y. Wang, Granular avalanche statistics in rotating drum with varied particle roughness, Natl. Sci. Open **2**, 20220069 (2023).

[20] H. Perrin, C. Clavaud, M. Wyart, B. Metzger, and Y. Forterre, Interparticle friction leads to nonmonotonic flow curves and hysteresis in viscous suspensions, Phys. Rev. X **9**, 031027 (2019).

[21] E. DeGiuli and M. Wyart, Friction law and hysteresis in granular materials, Proc. Natl. Acad. Sci. **114**, 9284 (2017).

[22] E. DeGiuli, J. N. McElwaine, and M. Wyart, Phase diagram for inertial granular flows, Phys. Rev. E **94**, 012904 (2016).

[23] O. Pouliquen and N. Renaut, Onset of granular flows on an inclined rough surface: Dilatancy effects, J. Phys. II **6**, 923 (1996).

[24] L. Staron, J.-P. Vilotte, and F. Radjai, Preavalanche instabilities in a granular pile, Phys. Rev. Lett. **89**, 204302 (2002).

[25] A. Amon, R. Bertoni, and J. Crassous, Experimental investigation of plastic deformations before a granular avalanche, Phys. Rev. E **87**, 012204 (2013).

[26] V. Y. Zaitsev, P. Richard, R. Delannay, V. Tournat, and V. E. Gusev, Pre-avalanche structural rearrangements in the bulk of granular medium: Experimental evidence, Europhys. Lett. **83**, 64003 (2008).

[27] I. S. Aranson and L. S. Tsimring, Patterns and collective behavior in granular media: Theoretical concepts, Rev. Mod. Phys. **78**, 641 (2006).

[28] L. Staron and F. Radjai, Friction versus texture at the approach of a granular avalanche, Phys. Rev. E **72**, 041308 (2005).

[29] L. Quartier, B. Andreotti, S. Douady, and A. Daerr, Dynamics of a grain on a sandpile model, Phys. Rev. E **62**, 8299 (2000).

[30] N. Xu and C. S. O'Hern, Measurements of the yield stress in frictionless granular systems, Phys. Rev. E **73**, 061303 (2006).

[31] H. Perrin, M. Wyart, B. Metzger, and Y. Forterre, Nonlocal effects reflect the jamming criticality in frictionless granular flows down inclines, Phys. Rev. Lett. **126**, 228002 (2021).

[32] See Supplemental Material at http://link.aps.org/supplemental/10.1103/PhysRevFluids.10.034301 for the sensitivity analysis.

[33] V. Smilauer *et al.*, Yade Documentation 3rd ed. The Yade Project (http://yade-dem.org/doc/) DOI:10.5281/zenodo.5705394.

[34] T. Schwager and T. Pöschel, Coefficient of restitution and linear–dashpot model revisited, Granular Matter **9**, 465 (2007).

[35] J.-N. Roux and G. Combe, Quasistatic rheology and the origins of strain, C. R. Phys. **3**, 131 (2002).

[36] A. Favier de Coulomb, M. Bouzid, P. Claudin, E. Clément, and B. Andreotti, Rheology of granular flows across the transition from soft to rigid particles, Phys. Rev. Fluids **2**, 102301(R) (2017).

[37] J. M. DallaValle, *Micrometrics: The technology of fine particles*, Vol. 2nd edition (Pitman Publishing Corp., 1948).

[38] R. Maurin, Investigation of granular behavior in bedload transport using an Eulerian-Lagrangian model, Ph.D. Thesis, Université Grenoble Alpes, 2015.

[39] O. Baran, D. Ertaş, T. C. Halsey, G. S. Grest, and J. B. Lechman, Velocity correlations in dense gravity-driven granular chute flow, Phys. Rev. E **74**, 051302 (2006).

[40] C. Cassar, M. Nicolas, and O. Pouliquen, Submarine granular flows down inclined planes, Phys. Fluids **17**, 103301 (2005).

[41] P. Jop, Y. Forterre, and O. Pouliquen, A constitutive law for dense granular flows, Nature (London) **441**, 727 (2006).

[42] P.-E. Peyneau and J.-N. Roux, Frictionless bead packs have macroscopic friction, but no dilatancy, Phys. Rev. E **78**, 011307 (2008).

[43] F. da Cruz, S. Emam, M. Prochnow, J.-N. Roux, and F. Chevoir, Rheophysics of dense granular materials: Discrete simulation of plane shear flows, Phys. Rev. E **72**, 021309 (2005).

[44] I. Srivastava, L. E. Silbert, G. S. Grest, and J. B. Lechman, Flow-arrest transitions in frictional granular matter, Phys. Rev. Lett. **122**, 048003 (2019).

[45] C. Lambert, Numerical analysis of hysteresis in granular media down inclined plane, Ph.D. Thesis, Université de Toulouse, 2024.

[46] R. A. Bagnold, The shearing and dilatation of dry sand and the 'singing' mechanism, Proc. R. Soc. London A **295**, 219 (1966).

[47] É. Azéma, F. Radjaï, and J.-N. Roux, Internal friction and absence of dilatancy of packings of frictionless polygons, Phys. Rev. E **91**, 010202(R) (2015).

[48] L. E. Silbert, D. Ertaş, G. S. Grest, T. C. Halsey, and D. Levine, Geometry of frictionless and frictional sphere packings, Phys. Rev. E **65**, 031304 (2002).

[49] L. E. Silbert, D. Ertaş, G. S. Grest, T. C. Halsey, and D. Levine, Analogies between granular jamming and the liquid-glass transition, Phys. Rev. E **65**, 051307 (2002).

[50] M. Wyart, On the dependence of the avalanche angle on the granular layer thickness, Europhys. Lett. **85**, 24003 (2009).

[51] C. Song, P. Wang, and H. A. Makse, A phase diagram for jammed matter, Nature (London) **453**, 629 (2008).